Proceedings of the All-Polish Seminar on Mössbauer Spectroscopy, Goniądz, Poland, June 17–20, 2018

Mössbauer Spectroscopy Studies of Fe-Doped $BaTiO_3$ Ceramics

E. Jartych[a,*], T. Pikula[a], B. Garbarz-Glos[b] and R. Panek[c]

[a]Lublin University of Technology, Institute of Electronics and Information Technology, Nadbystrzycka 38A, 20-618 Lublin, Poland

[b]Pedagogical University of Cracow, Institute of Technology, Podchorążych 2, 30-084 Cracow, Poland

[c]Lublin University of Technology, Department of Geotechnics, Civil Engineering and Architecture Faculty, Nadbystrzycka 40, 20-618 Lublin, Poland

The Fe-doped $BaTiO_3$ ceramics with various iron concentration were prepared by the conventional ceramic technology. Structure of the samples was studied by X-ray diffraction, scanning electron microscopy and energy-dispersive X-ray spectroscopy. Hyperfine interactions were determined using the Mössbauer spectroscopy. As confirmed by structural investigations, the obtained materials are good quality ceramics, homogeneous and free of iron oxides and Fe dopant clustering. It was found that Fe ions are incorporated into the tetragonal lattice of barium titanate, which is accompanied by the formation of oxygen vacancies. Paramagnetic behavior of Fe-doped $BaTiO_3$ was observed in the Mössbauer spectra at room temperature as a superposition of singlet and two doublets. These components originate from Fe^{3+} ions which substitute Ti^{4+} ions at octahedral sites inside of less or more distorted oxygen octahedrons and at pentahedral sites, i.e., inside octahedrons with no one oxygen ion.

DOI: 10.12693/APhysPolA.134.1058

PACS/topics: 81.05.Je, 61.05.cp, 76.80.+y, 31.30.Gs

1. Introduction

Because multiferroics (in which ferromagnetism and ferroelectricity coexist in the same phase and at room temperature) are quite rare in nature, scientists are trying to create such materials in the laboratory. One way is doping of the most known ferroelectric material, i.e., barium titanate $BaTiO_3$ with perovskite ABO_3 structure. Ferromagnetism in this compound may be achieved by doping A or B sites with magnetic ions. In particular, the Fe-doped $BaTiO_3$ system has attracted much attention of experimentalists and theoreticians in the last years [1–3].

Doping affects the crystal structure of pure barium titanate which typically has a tetragonal lattice at room temperature. The final structure depends not only on the doping level but also on the preparation conditions. At high doping levels, between 20 and 70% (molar fraction), the phase structure of Fe-doped $BaTiO_3$ ceramics is hexagonal when it is prepared by solid-state sintering at 1200 or 1300 °C [1, 2, 4]. For low doping levels, the room-temperature structure of Fe-doped $BaTiO_3$ may be tetragonal (when the iron concentration is ≈ 1 mol% [5]), mixed tetragonal and hexagonal (for doping levels from 2 to 10 mol% [6, 7], or 7–12 mol% [8]) or tetragonal-pseudocubic when the Fe content is 3 mol% (prepared from commercial $BaTiO_3$ nanoparticles and iron particles smaller than 1 μm [9]).

The intrinsic capability of ABO_3 structure to host ions of different size allows accommodating a large number of various dopants in the $BaTiO_3$ lattice. When a trivalent ion substitutes the Ti site it behaves as an acceptor whereas the substitution at the Ba site enables the donor conductivity. For transition metals, like Cr, Co, Fe and Ni, it is well established and accepted that they preferentially substitute the Ti site. Incorporation of Cr^{4+} does not require charge compensation, whereas incorporation of Ni^{2+}, Fe^{3+}, Co^{3+} is compensated by the formation of oxygen vacancies [5]. Doping $BaTiO_3$ affects structural changes and is intended to improve electrical properties [10–12]. Very recently, giant dielectric permittivity of 66650 at 1 kHz (19 times higher than that for the un-doped barium titanate) together with the relatively low dielectric loss tangent of 0.13 were reported for Fe-doped $BaTiO_3$ ceramics with 5 mol% Fe content [9]. Such high value of dielectric permittivity was explained as induced by the interfacial polarization between insulating $BaTiO_3$ ferroelectrics and semiconducting iron oxides with mixed-valence structure of Fe^{2+}/Fe^{3+} states (confirmed by X-ray photoelectron spectroscopy).

In the present work, the Mössbauer spectroscopy was used to study the hyperfine interactions in Fe-doped $BaTiO_3$ compound. Ceramic samples $BaTiO_3 + x$ wt% Fe_2O_3 ($x = 1$, 2, and 3%) were prepared by a solid-state synthesis. Low doping concentrations were selected because there is little data in the literature about the influence of a small amount of Fe dopant on barium titanate properties. X-ray diffraction (XRD) and scanning electron microscopy (SEM) were applied to learn the structure of the material. The main goal of the studies was to determine the oxidation state of iron and nearest neighborhood of Fe ions incorporated into the $BaTiO_3$ lattice.

*corresponding author; e-mail: e.jartych@pollub.pl

2. Experiment

The $BaTiO_3$ + x wt% Fe_2O_3 ceramics (for $x = 1$, 2 and 3%) were prepared by solid-state reaction. The samples were synthesized from analytically pure titanium oxide TiO_2, iron oxide Fe_2O_3 and barium carbonate $BaCO_3$. The mixture of starting raw materials was homogenized and ground in an agate ball mill in ethanol for 24 h, dried and then calcined in a crucible for 1.5 h at the temperature 1350 °C. After the calcination the powder was ground in ethanol, cold pressed (under 100 MPa pressure), and sintered for 1 h with the use of a conventional ceramic technology at the temperature 1450 °C.

XRD studies were performed at room temperature using PANalytical X-Pert Pro diffractometer equipped with Cu lamp. The phase and structural analyses of the registered XRD patterns were made with the X'Pert High-Score Plus computer program on the ICDD PDF2 database. SEM investigations were carried out with a field emission Hitachi S4700 scanning electron microscope equipped with an energy-dispersive X-ray spectroscopy (EDS) Noran Vantage system. The investigations of microstructure of polycrystalline specimens were performed on polished sections and fractures. Before the measurements the samples were sputtered with carbon in order to carry away the electric charge from the surface. The homogeneity of the samples composition and distribution of elements at the samples surface were checked using the EDS and electron probe microbeam analysis (EPMA). ^{57}Fe Mössbauer spectra were recorded at room temperature using POLON spectrometer working at a constant acceleration mode in a transmission geometry. A source of ^{57}Co (in a rhodium matrix) with an activity of 50 mCi was used. All values of isomer shift within this paper are related to the α-Fe standard.

3. Results and discussion

Results of the analysis of chemical compositions made in the chosen micro-regions of the surface of $BaTiO_3$ + x wt% Fe_2O_3 ceramic samples are shown in Fig. 1. The EDS spectra show that all samples contain Ba, Ti, O and Fe elements near their surfaces. The peak from carbon visible in all spectra is connected with sputtering of the sample surface before measurements. In EDS spectra nothing more than peaks from the expected elements are seen which confirms the purity of the samples. The assumed qualitative composition was achieved. An actual Fe concentrations in the samples are: 0.79, 1.58, and 2.35 wt% (0.64, 1.25, and 1.78 at.%, respectively).

The homogeneity of elements distribution on the polished surface of the samples was checked using EPMA in the mapping mode (Fig. 2). The obtained "mappings" confirmed the qualitative composition of the obtained samples and exhibited homogeneous distribution of the Ba, Ti, O and Fe elements.

In Fig. 3 SEM micrographs of the fractures of $BaTiO_3$ + x wt% Fe_2O_3 ceramics for $x = 1$, 2 and 3% in magnification 10000× are presented. The fracture has a fragile nature and in the grains a tendency to the formation of crystalline structure is observed. Larger grains coexist with the smaller ones and with a certain amount of intergranular pores. The average grain size of doped $BaTiO_3$ is about 2.5 μm. A good homogeneity of the microstructure and a small degree of porosity may be noted. For the reference sample, i.e., un-doped $BaTiO_3$ well-crystallized grains with the average size of about 15 μm and rounded shape are visible (Fig. 4).

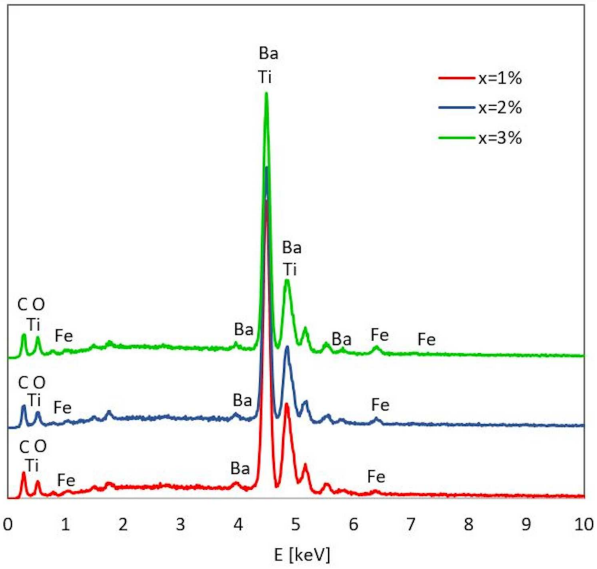

Fig. 1. The results of EDS analysis of $BaTiO_3$ + x wt% Fe_2O_3 ceramics for $x = 1$, 2, and 3%.

It may be concluded that doping with Fe ions affects the microstructure of barium titanate and leads to the decrease of grain size. This observation is in agreement with the literature data for $BaTiO_3$ doped with hafnium [13] or iron [14].

XRD patterns registered for the samples of $BaTiO_3$ + x wt% Fe_2O_3 ceramics for $x = 1$, 2, and 3% are shown in Fig. 5. No signals corresponding to α-Fe, α-Fe_2O_3, γ-Fe_2O_3 or Fe_3O_4 were detected in any of the samples. Small amount of secondary phase, i.e., $Ba_4Ti_{11}O_{26}$ was recognized for all samples (low intensity diffraction lines at 2Θ angles 27 and 30° in Fig. 5, ICSD Card No. 01-083-1459). As reported in the literature, for low doping concentrations of Fe to $BaTiO_3$, the tetragonal structure of the material is expected. In the case of our samples, all diffraction lines fit well to both tetragonal $P4mm$ phase (ICSD Card No. 01-073-1282) and orthorhombic $Amm2$ phase (ICSD Card No. 01-081-2200). However, using the Rietveld refinement method, the best numerical fit of the XRD patterns was achieved assuming the tetragonal $P4mm$ structure.

The determined lattice parameters are listed in Table 1. It may be noted, that in comparison to the lattice parameters of pure $BaTiO_3$ ($a = b = 3.9941$ Å and $c = 4.0335$ Å [14]) the values of a, b, c increase or decrease when the dopant Fe concentration increases.

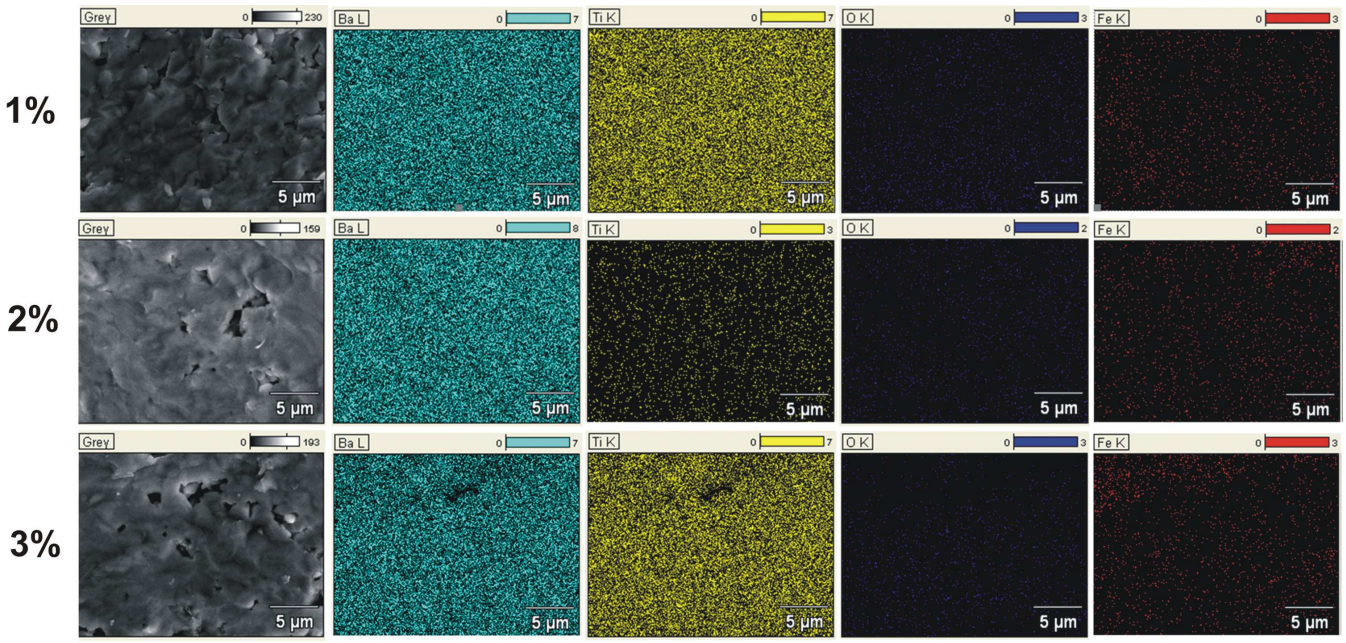

Fig. 2. Microstructure and distribution of the main components (mapping) in $BaTiO_3$ + x wt% Fe_2O_3 ceramics for $x = 1$, 2 and 3%.

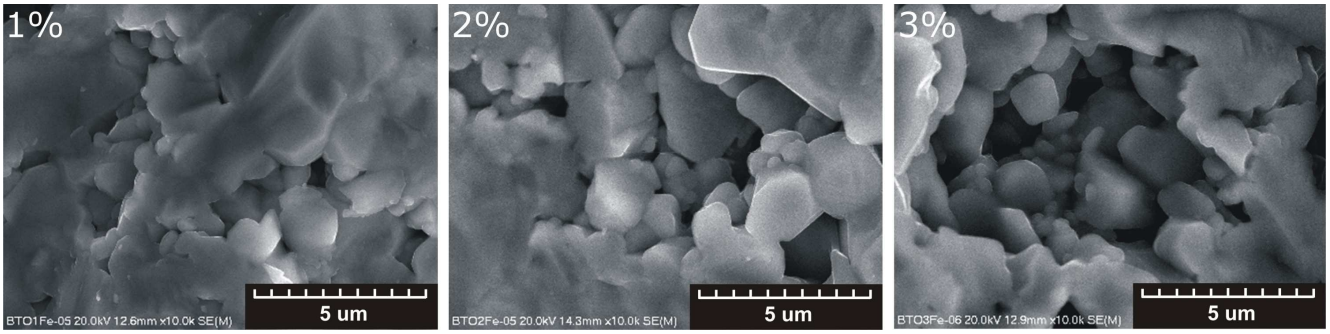

Fig. 3. SEM micrographs of the fractured surface of $BaTiO_3$ + x wt% Fe_2O_3 ceramics for $x = 1$, 2 and 3% (magnification 10000×).

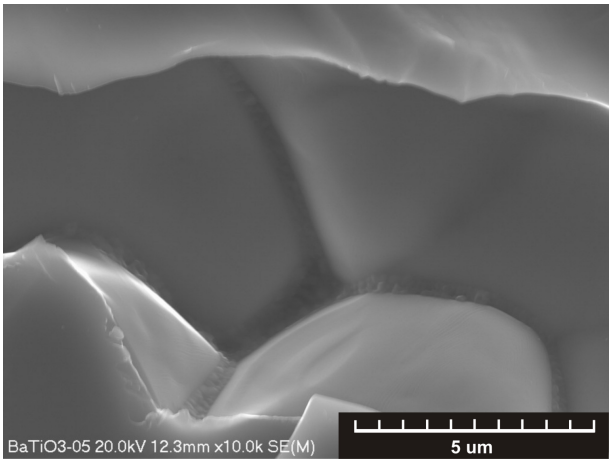

Fig. 4. SEM micrograph of the fractured surface of undoped $BaTiO_3$.

The substitution site is mainly determined by ionic radius and charge. Based on the difference in ion size (for Fe^{3+} ions 0.064 nm and for Ti^{4+} ions 0.0605 nm for the coordination number 6 [15]), substitution of Fe^{3+} for Ti^{4+} could enlarge the lattice constant. However, the electric charge of Fe^{3+} ions is different from that of Ti^{4+} ions and doping with Fe^{3+} ions results in formation of oxygen vacancies. In turn, oxygen vacancies may induce the lattice shrinkage. Thus, the observed lattice distortions in our samples are result of competition effect among these two factors, i.e., radius and charge.

Results of the Mössbauer spectroscopy studies are presented in Figs. 6 and 7. Spectra were measured in a large and small scale of the source velocity. From Fig. 6 (the sample with 3 wt% Fe_2O_3 was chosen as an example) it may be noted that there are no traces of six-line components, thus the existence of α-Fe, α-Fe_2O_3, γ-Fe_2O_3 or Fe_3O_4 phases in Fe-doped $BaTiO_3$ ceramics may be

TABLE I

Structural parameters of $BaTiO_3$ + x wt% Fe_2O_3 ceramics for x = 1, 2 and 3%; a, b, c, α, β, γ — lattice parameters.

Nominal content of Fe_2O_3 [wt%]	Actual content of Fe [at.%]	$a = b$ [Å]	c [Å]	$\alpha = \beta = \gamma$ [°]
1	0.64	3.998(1)	4.032(1)	90
2	1.25	4.001(1)	4.036(1)	90
3	1.78	3.998(1)	4.031(1)	90

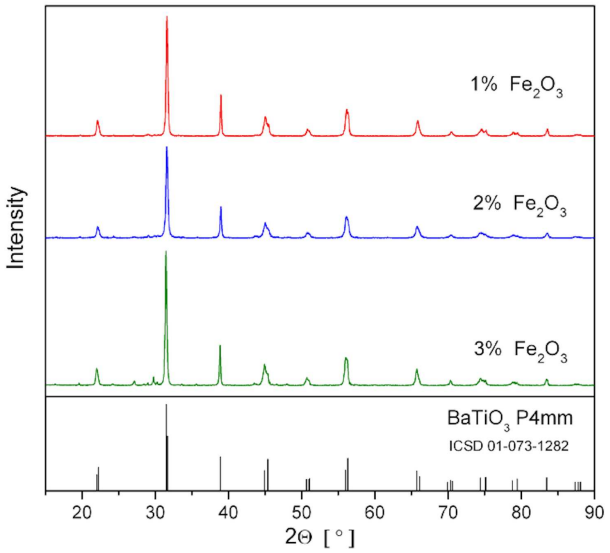

Fig. 5. XRD patterns of $BaTiO_3$ + x wt% Fe_2O_3 ceramics for x = 1, 2 and 3%.

ruled out. For all concentrations of Fe dopant Mössbauer spectra have double-line shape. Numerical fitting was performed by use of discrete components, i.e., single line (S) and two doublets ($D1$ and $D2$). The hyperfine interactions parameters of the components are listed in Table II. The values of isomer shift for all components are about 0.3 mm/s and confirm that iron ions are in 3+ state. There is no trace of the component with high value of isomer shift ($\approx$ 1 mm/s), thus the existence of Fe^{2+} ions in the samples may be excluded.

In the applied model, the singlet S (black line Fe^{3+} octa-Ti in Fig. 7) may indicate Fe^{3+} ions which replace Ti in the octahedrons having high symmetry, thus the corresponding quadrupole splitting should be zero [4]. The contribution of singlet decreases with an increase of iron content (Table II). For higher doping concentration, symmetry of octahedra could be lowered (the quadrupole splitting is no longer zero) and the contribution of such distorted octahedral sites (doublet $D1$, magenta line Fe^{3+} octa-Ti, Fig. 7) increases. The second doublet $D2$ (orange line Fe^{3+} penta-Ti, Fig. 7) is assigned to Fe^{3+} ions in the pentahedral sites. The pentahedral sites are sites in the center of oxygen octahedra without one oxygen atom because when Ti^{4+} is substituted by Fe^{3+}, oxygen

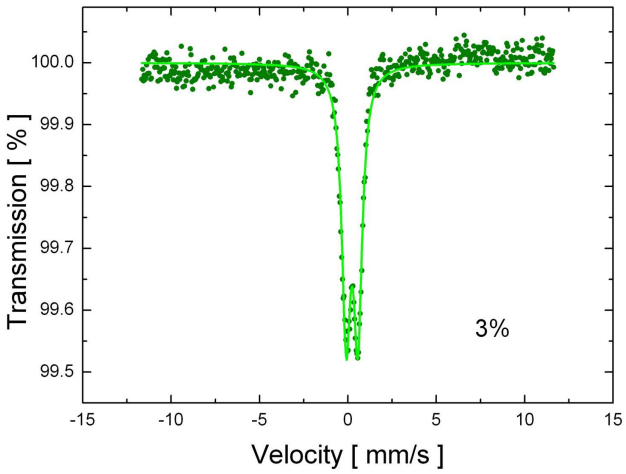

Fig. 6. Room-temperature Mössbauer spectrum recorded in a large velocity scale for $BaTiO_3$ + 3 wt% Fe_2O_3 ceramics.

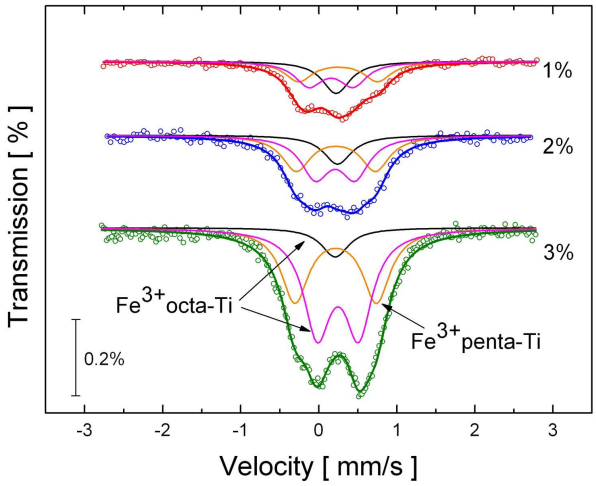

Fig. 7. Room-temperature Mössbauer spectra recorded in a small velocity scale for $BaTiO_3$ + x wt% Fe_2O_3 ceramics for x = 1, 2 and 3%.

vacancies are created to maintain electro-neutrality condition. Lack of oxygen ions in octahedra causes further lattice distortion and increase in electric field gradient. Thus, the quadrupole splitting of doublet $D2$ has high value. The obtained results are in good agreement with data reported in [1, 2, 4].

4. Conclusions

The solid-state reaction was successfully used to prepare Fe-doped $BaTiO_3$ ceramics. XRD, EDS, EPMA, and MS results proved that Fe dopant is incorporated into the $BaTiO_3$ structure. The analysis of the obtained results suggests that Fe-doped $BaTiO_3$ samples are homogeneous and free of iron oxides and Fe dopant clustering. The Fe-doped $BaTiO_3$ ceramics has tetragonal structure; however, higher doping concentration caused formation of $Ba_4Ti_{11}O_{26}$ secondary phase.

TABLE II

Hyperfine interactions parameters of $BaTiO_3$ + Fe_2O_3 ceramics derived from room-temperature Mössbauer spectra: δ — isomer shift relative to α-Fe standard, Δ — quadrupole splitting, Γ — half width at half maximum of spectral lines, χ^2 — fitting parameter, A — relative area of the component; uncertainties are given in brackets for the last significant number.

Nominal content of Fe_2O_3 [wt%]	Actual content of Fe [at.%]	δ [mm/s]	Δ [mm/s]	Γ [mm/s]	χ^2	A [%]	Component
1	0.64	0.32(1)	–	0.21(1)	1.0	27	S octa-Ti
		0.26(3)	0.56(2)			40	$D1$ octa-Ti
		0.35(2)	1.01(3)			33	$D2$ penta-Ti
2	1.25	0.34(1)	–	0.21(1)	0.9	16	S octa-Ti
		0.31(2)	0.50(2)			45	$D1$ octa-Ti
		0.32(2)	1.01(2)			39	$D2$ penta-Ti
3	1.78	0.31(2)	–	0.21(1)	1.2	8	S octa-Ti
		0.35(1)	0.53(2)			53	$D1$ octa-Ti
		0.32(2)	1.04(2)			39	$D2$ penta-Ti

Fe ions in $BaTiO_3$ structure do not order magnetically. The values of isomer shifts prove the third oxidation state of iron. The Mössbauer spectroscopy revealed substitution of octahedral and pentahedral Ti sites by Fe^{3+} ions in the tetragonal lattice of $BaTiO_3$.

References

[1] F. Lin, D. Jiang, X. Ma, W. Shi, *J. Magn. Magn. Mater.* **320**, 691 (2008).

[2] F. Lin, W. Shi, *Physica B* **407**, 451 (2012).

[3] J.J. Meléndez, Y.A. Zulueta, Y. Leyet, *Ceram. Int.* **41**, 1647 (2015).

[4] E. Mashkina, C. Mccammon, F. Seifert, *J. Solid State Chem.* **177**, 262 (2004).

[5] M.T. Buscaglia, V. Buscaglia, M. Viviani, P. Nanni, M. Hanuskova, *J. Eur. Ceram. Soc.* **20**, 1997 (2000).

[6] S. Qiu, W. Li, Y. Liu, G. Liu, Y. Wu, N. Chen, *Trans. Nonferrous Met. Soc. China* **20**, 1911 (2010).

[7] A. Rani, J. Kolte, S.S. Vadla, P. Gopalan, *Ceram. Int.* **42**, 8010 (2016).

[8] N.V. Dang, N.T. Dung, P.T. Phong, I.J. Lee, *Physica B* **457**, 103 (2015).

[9] B. Luo, X. Wang, E. Tian, H. Song, Q. Zhao, Z. Cai, W. Feng, L. Li, *J. Eur. Ceram. Soc.* **38,** 1562 (2018).

[10] D. Sitko, W. Bąk, B. Garbarz-Glos, A. Budziak, C. Kajtoch, A. Kalvane, *IOP Conf. Series: Mat. Sci. Eng.* **49**, 012050 (2013).

[11] W. Bąk, P. Dulian, D. Sitko, B. Garbarz-Glos, C. Kajtoch, K. Wieczorek-Ciurowa, I. Smeltere, *Ferroelectrics* **464**, 35 (2014).

[12] D. Sitko, B. Garbarz-Glos, M. Livinsh, W. Bąk, M. Antonova, C. Kajtoch, *Ferroelectrics* **486**, 8 (2015).

[13] B. Garbarz-Glos, W. Bąk, A. Molak, A. Kalvane, *Phase Transit.* **86** (2013).

[14] Z. Yu, X.Chen, *J. Electron. Mater.* **47**, 3459 (2018).

[15] *CRC Handbook of Chemistry and Physics*, Ed. D.R. Lide, 87th ed., CRC Press, 2006.